

# Micro-scale modeling of anisotropy effects on undrained behavior of granular soils

Z. X. Yang · J. Yang · L. Z. Wang

Received: 7 February 2013 / Published online: 3 July 2013  
© Springer-Verlag Berlin Heidelberg 2013

**Abstract** This paper presents a micro-scale modeling of fabric anisotropy effects on the mechanical behavior of granular assembly under undrained conditions using discrete element method. The initial fabrics of the numerical samples engendered from the deposition under gravity are measured, quantified and compared, where the gravitational field can be applied in different directions to generate varying anisotropy orientations. The samples are sheared under undrained biaxial compression, and identical testing conditions are applied, with samples having nearly the same anisotropy intensities, but with different anisotropy directions. The macroscopic behaviors are discussed for the samples, such as the dilatancy characteristics and responses at the critical state. And the associated microstructure changes are further examined, in terms of the variables in the particulate scale, with the focus on the fabric evolution up to a large deformation reaching the critical state. The numerical analysis results compare reasonably well with available experimental data. It is also observed that at critical state, in addition to the requirements by classical critical state theory, a unique fabric structure has also been developed, and might be independent of its initial fabric. This observation is coincided with the recent theoretical achievement of anisotropic critical state theory. Finally,

a general framework is introduced for quantifying and modeling the anisotropy effects.

**Keywords** Fabric anisotropy · Bedding plane · Principal stress direction · Critical state · Granular materials

## Abbreviations

$\alpha$	Bedding angle with respect to horizontal axis during gravitational deposition of sample preparation
$\sigma_x, \sigma_y$	Principal stresses along $x$ and $y$ directions respectively
$p, q$	Mean normal stress and deviatoric stress respectively
$CN$	Coordination number
$\varepsilon_a$	Axial strain along $y$ direction
$D$	Dilatancy
$\varepsilon_v^p, \varepsilon_q^p$	Plastic volumetric and deviatoric strains respectively
$F_{ij}$	Fabric tensor
$F'_{ij}$	Fabric tensor by an orthogonal rotation
$\vartheta$	Orthogonal rotation angle of fabric tensor
$F_{11}, F_{22}, F_{12}$	Components of fabric tensor $F_{ij}$ in two-dimension
$F_1, F_2$	Principal values of fabric tensor $F_{ij}$
$\Delta, \varphi$	Intensity and principal direction (with respect to horizontal axis) of fabric tensor $F_{ij}$
$\Delta^p, \varphi^p$	Intensity and principal direction fabric tensor $F_{ij}$ in terms of particle orientation
$\Delta^c, \varphi^c$	Intensity and principal direction fabric tensor $F_{ij}$ in terms of contact unit normal
$\Delta^b, \varphi^b$	Intensity and principal direction fabric tensor $F_{ij}$ in terms of branch vector orientation
$\mu$	Inter-particle friction

Z. X. Yang (✉) · L. Z. Wang  
Department of Civil Engineering, Research Center of Coastal and Urban Geotechnical Engineering, Zhejiang University, Hangzhou, China  
e-mail: zxyang@zju.edu.cn

L. Z. Wang  
e-mail: wanglz@zju.edu.cn

J. Yang  
Department of Civil Engineering, The University of Hong Kong, Hong Kong, China  
e-mail: junyang@hku.hk

$\sigma_{ij}, \widehat{\sigma}_{ij}$	Stress tensor and deviatoric direction of stress tensor respectively
$A$	Anisotropic state parameter

## 1 Introduction

Granular media like sand, due to the influence of gravitational force during the deposition process, may possess initial fabric anisotropy. Ample experimental evidence has shown the significance of the impact of the initial fabric anisotropy on the mechanical behavior of granular materials, and have been reported widely [1–5]. Among these studies, two are of general interests. One is that an initially anisotropic sand may behave dramatically differently when undergone loading with distinct principal stress directions in reference to the material's axes of anisotropy, whereas otherwise identical conditions [2,3]. The other is that the samples composed of the same material but prepared by different methods also exhibit strikingly different responses under the same loading path [5–9].

However, it is noted that a direct assessment or measurement on the fabric anisotropy (either initial or induced) [10], is scarce in most of the research. To understand how the fabric evolves and also the role that the fabric played in soil mechanics, as argued in academics, may be of great significance to disclosing the well-accepted critical state theory [1,11–13]. As pointed out by Li and Dafalias [14], a unique critical-state line for a soil may be relevant to a unique structure at the critical state, which is essentially independent of the soil initial fabric on loading history. They contend that at the critical state, the initial material fabric as well as the memory of the loading history has essentially been erased after experiencing a very large shear deformation. This argument has been proven recently in the perspective of the thermodynamics theory; see Li and Dafalias [13].

Nevertheless, it is well acknowledged that to quantify the fabric anisotropy for a granular material is still not easy, especially in examining the fabric evolution under loading stage. Some earlier experimental investigations [5,15–17] involved preserving the fabric of the specimens with epoxy, cutting small patches, and using microscopy to study the microstructure of sandy soils. To quantify the microstructure changes, Oda et al. [18,19], Calvetti et al. [20] and Wood and Leśniewska [21] used photoelastic rods to form the tested sample and assessed the micro fabric changes by optical methods. More recently, computed tomography (CT) has emerged as a powerful tool to obtain high-quality image of tested sample during the loading process [22–25]. Particularly, the microstructure evolution and shear band development during the loading can be well quantified by X-ray CT technique; see Oda et al. [26] and Takemura et al. [27].

Aside from physical examination of the fabric evolutions, it can alternatively be investigated numerically using discrete element method (DEM). As a numerical tool, DEM treats the granular material as an assembly of particles that interact via a contact logic, tracks translation and rotation of each particle and can offer a thorough perspective of the overall behaviors as well as the response at the particulate level. Efforts have been made in recent year to link the macro-scale and critical state behavior with the micro-scale analyses by DEM. Nougier-Lehon et al. [28] presented a numerical analysis by DEM biaxial tests, of the influence of particle shape on the critical state, and the existence of critical anisotropy for various particle shapes and different loading directions was also investigated. By performing a series of biaxial compression tests using DEM, Rotherburg and Kruyt [29] suggested that critical state theory should be interpreted in terms of both the fabric anisotropy and coordination number at the critical state of the granular materials. Cheng et al. [30] investigated the uniqueness of critical states with crushable grains using DEM, and found that grain crushing led 'critical state' to an ambiguous concept. 2D shear cell tests using polygonal particles by Peña et al. [31], showed the significant influence of particle shape on the global mechanical behavior of dense granular media, and the corresponding micromechanical level interpretation of the role of particle shape was presented, along with the critical state anisotropy analyses. Peña et al. [32] proved samples with different initial densities would approach a unique critical state under biaxial compression using polygonal particles, even with a wide range of inter-particle friction coefficients, but some unstable and fluctuations may existed at the critical state, which was interpreted as micro-structure rearrangements in the granular system.

This paper describes a DEM-based analysis on the micro-mechanical behavior of initially anisotropic granular materials and discusses the fabric anisotropy (and its evolution) and also the role that played in the mechanical response. The focus is placed on the fabric evolution and its relation to the critical state. To quantify and simulate the effects of the fabric anisotropy on the behavior of the granular assembly, a joint tensor based general framework is introduced to address the effects by both the material's fabric and principal stress orientation.

## 2 Numerical implementation

DEM assumes the material consisting of separate, discrete particles and is particularly capable of describing the micro-mechanical behavior of granular assemblies. In this study, a commercial code *PFC*<sup>2D</sup> (Particle Flow Code in 2-D) [33] based on DEM proposed by Cundall and Strack [34] is employed. In the code, an explicit time-stepping numerical

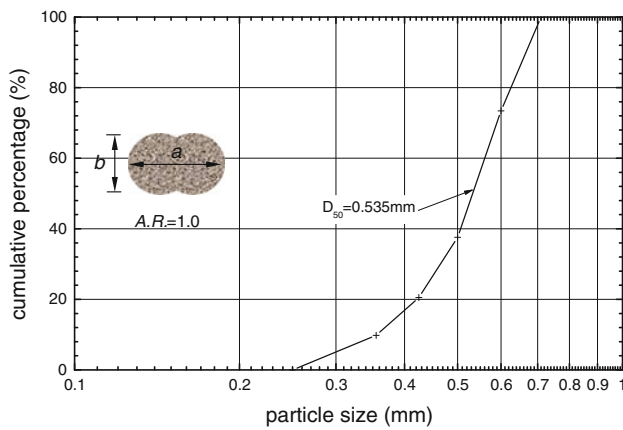


**Fig. 1** Grading curve of the numerical sample

scheme is implemented and the motion of individual particles is traced and contacts with neighboring particles are updated according to a particular contact law. A detailed description on the theory and background can be referred to Cundall and Strack [34].

To consider more realistic particle shape, the clumped particle is adopted to generate the assembly; each constituent particle is formed by glueing and overlapping two identical basic disk particles and behaves as a rigid body that will not break apart, regardless of the forces acting upon it. The particle volume/area is varying with the ‘base’ disk particles and overlapping extent. In this study, the size of the ‘base’ disk particles are 0.26–0.66 mm in diameter and the clumped particle has a constant aspect ratio (AR)=0.6, which is defined to characterize the shape of clumped particle as shown in Fig. 1. The sample equivalent particle diameter, defined as the diameter of the circular particle with the same area as the clumped particle, falls also in the range of 0.26 and 0.66 mm. The resulting particle grading curve is illustrated in Fig. 1, with  $d_{50} = 0.535 \text{ mm}$ . Unlike the circular particle, the clumped particle has its distinct orientation, i.e. the direction of long axis.

The numerical sample is generated using deposition method, which allows the particles to settle freely in place under gravity as illustrated in Fig. 2, very similar to the sample preparation method for sand in the laboratory [35]. The sample prepared by this method has distinct initial fabric anisotropy due to the apparent bedding plane. If the gravitational force is applied upon in different angles to the horizontal direction, the bedding plane is in different orientation and thus material’s fabric anisotropy. It is emphasized that particle orientation is not an essential measure of fabric anisotropy of materials, which implies that if particles do not have a preferred axis, the sample formed spherical/round particles could still be anisotropic as long as the packing would be anisotropic.

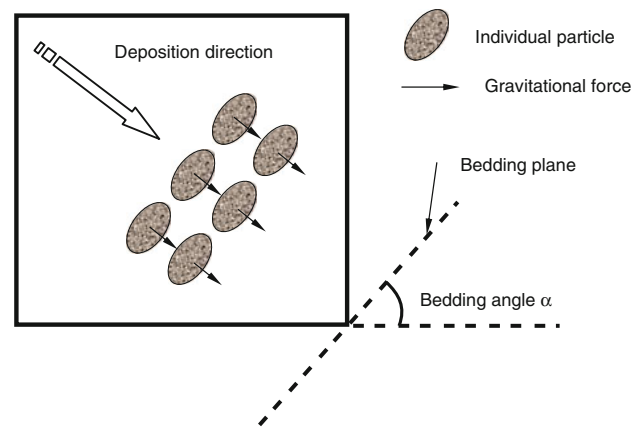


**Fig. 2** Creation of the numerical sample under gravitational force

Figure 3 illustrates the procedures of the sample generation. Particles are firstly generated with random orientations in a bounded rectangular area (50 mm × 50 mm). With reference to the inclination of the bedding plane, a gravitational acceleration can be applied to force the particles deposit perpendicularly to the bedding plane. It is noted that during the sample generation process, temporarily assigned inter-particle friction is helpful to control the density of the sample. Once all the particles have been deposited and the whole system reaches an equilibrium state, the lower right part with a dimension of 25 mm × 25 mm (Fig. 3b, c) is trimmed as the test sample. The sample is applied with boundary conditions given in Fig. 4, and is assigned with a normal inter-particle friction  $\mu = 0.5$  afterwards. Other parameters for the linear spring-slider (normal and tangent bi-directional linear spring and tangent Coulomb-type slip model) contact law used in this study are summarized in Table 1.

Prior to the shearing, each sample will be isotropically compacted to the desired stress state. Then, the sample is sheared under constant volume condition, which is presumably equivalent to the ‘undrained’ shear test for saturated soil. In the test, the equivalent ‘excess pore water pressure’ is the variation in the lateral normal stress; such that both the vertical and horizontal stresses derived from DEM simulations are in terms of effective stress, as they are transmitted through the inter-particle contacts; see Yimsiri and Soga [36]. As shown in Fig. 4, the deviatoric load is applied in a strain-control manner, by simultaneously pushing the upper and lower walls inward the sample with a very small loading rate, while the position of lateral walls is adjusted accordingly to satisfy no volumetric change condition.

### 3 Initial anisotropy quantification

The geometrical packing of particles with associated voids contributes to the general feature: fabric anisotropy, for

**Fig. 3** Numerical sample generation procedure. **a** Deposition under inclined gravity, **b** equilibrium state after deposition, **c** numerical sample by partition

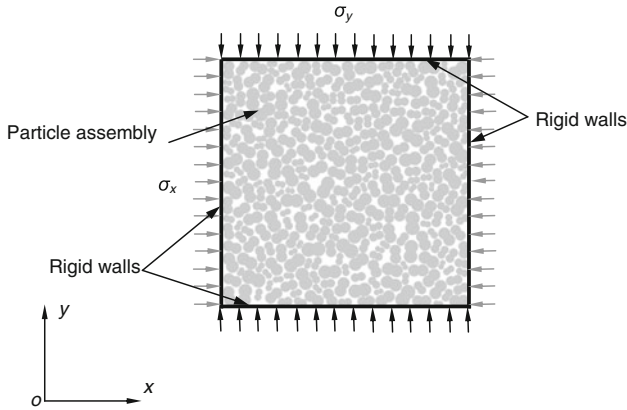
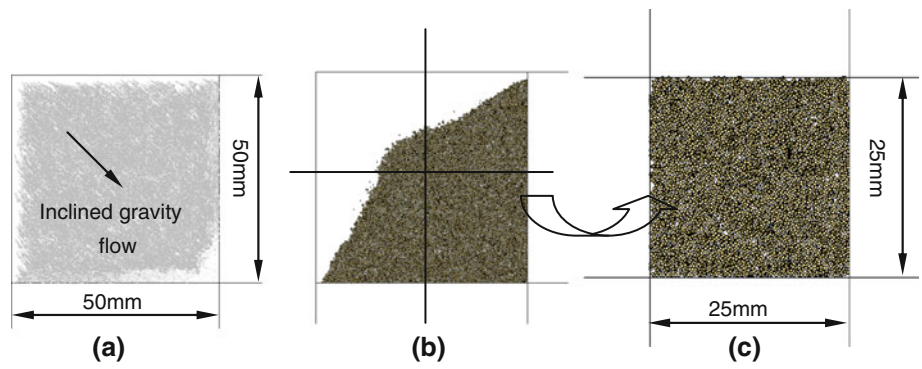


**Fig. 4** A numerical sample with boundary conditions

**Table 1** parameters used in numerical simulations

Mass density (kg/m <sup>2</sup> )	Normal/tangential stiffness of particle (N/m)/wall	Particle/wall friction	Damping parameter
2,600	10 <sup>9</sup>	0	0.7

granular materials. It is often to use the micro-scale variables to quantify their fabrics, including particle orientation, contact unit normal and branch vector orientation that can be characterized by a pair of unit vectors **n** and **-n**, with opposite directions. Figure 5 defines the representations of these micro-scale variables in a granular assembly. A fabric tensor **F** can be expressed in a general form [37]:

$$F_{ijlm\dots} = \frac{1}{2N} \sum_{k=1}^{2N} n_i^k n_j^k n_l^k n_m^k \dots \quad (1)$$

where  $2N$  is the total number of the measurements, the superscript  $k$  denotes the  $k$ th unit vectors among  $2N$ , and  $n_i^k$  ( $i=1,2,3$ ) are three direction cosines of the unit vector  $\mathbf{n}^k$  with respect to the reference axes  $x_i$  ( $i = 1, 2, 3$ ) in a Cartesian coordinate system. However, a spherical coordination system is often used and shown in Fig. 6. In this coordination system, the second order fabric tensor can be explicitly expressed into

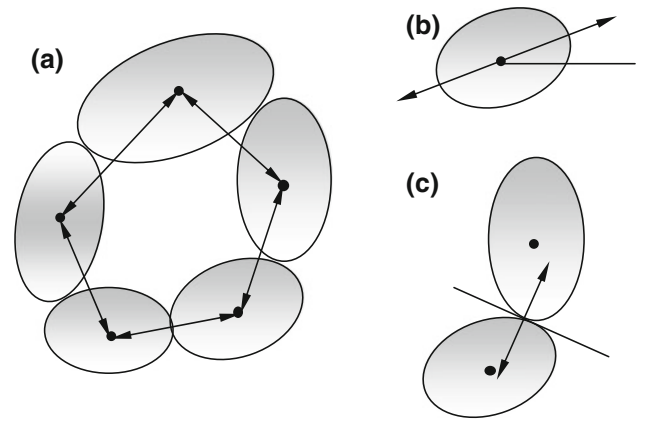


**Fig. 5** Micro-quantities in a granular assembly. **a** Branch vector, **b** particle orientation, **c** contact unit normal

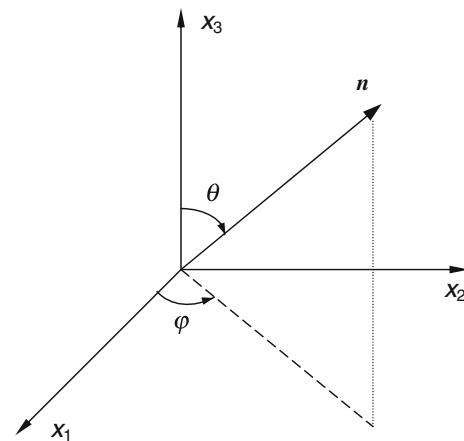


**Fig. 6** A spherical coordinate system

$$F_{ij} = \begin{pmatrix} F_{11} & F_{12} & F_{13} \\ F_{21} & F_{22} & F_{23} \\ F_{31} & F_{32} & F_{33} \end{pmatrix} = \frac{1}{2N} \times \begin{pmatrix} \sum \sin^2 \theta^k \cos^2 \varphi^k & \sum \sin^2 \theta^k \cos \varphi^k \sin \varphi^k & \sum \sin \theta^k \cos \theta^k \cos \varphi^k \\ \sum \sin^2 \theta^k \cos \varphi^k \sin \varphi^k & \sum \sin^2 \theta^k \sin^2 \varphi^k & \sum \sin \theta^k \cos \theta^k \sin \varphi^k \\ \sum \sin \theta^k \cos \theta^k \cos \varphi^k & \sum \sin \theta^k \cos \theta^k \sin \varphi^k & \sum \cos^2 \theta^k \end{pmatrix} \quad (2)$$

Particularly, for 2-D case, the fabric tensor can be further reduced into the form

**Table 2** Summary of initial conditions of biaxial tests on ‘loose’ samples

Bedding angle $\alpha$ ( $^\circ$ )	Void ratio $e$	Orientational initial fabric		Contact unit normal initial fabric		Branch vector orientation	
		$\Delta^p$	$\varphi^p$	$\Delta^c$	$\varphi^c$	$\Delta^b$	$\Phi^b$
0	0.216	0.369	0.0	0.228	91.2	0.108	89.9
30	0.216	0.287	24.9	0.174	109.0	0.087	105.2
45	0.215	0.263	43.5	0.176	132.2	0.094	135.0
60	0.217	0.285	62.3	0.202	152.8	0.123	152.3
90	0.216	0.369	89.6	0.228	1.2	0.108	179.9

$$F_{ij} = \begin{pmatrix} F_{11} & F_{12} \\ F_{21} & F_{22} \end{pmatrix} = \frac{1}{2N} \begin{pmatrix} \sum \cos^2 \varphi^k & \sum \cos \varphi^k \sin \varphi^k \\ \sum \cos \varphi^k \sin \varphi^k & \sum \sin^2 \varphi^k \end{pmatrix} \quad (3)$$

In general, the off-diagonal components of  $F_{ij}$  do not vanish, and through certain tensor transformation, the principal values of  $F_{ij}$ ,  $F_1$  and  $F_2$  are given by

$$F_{1,2} = 1/2(F_{11} + F_{22}) \pm \sqrt{1/4(F_{11} - F_{22})^2 + F_{12}^2} = 1/2(1 \pm \Delta) \quad (4)$$

where  $\Delta = \sqrt{1/4(F_{11} - F_{22})^2 + F_{12}^2}$  is a measure of intensity of fabric anisotropy. By substituting of the corresponding components of  $F_{ij}$ , it can be expressed as

$$\Delta = \frac{1}{2N} \sqrt{(\sum \cos 2\varphi^k)^2 + (\sum \sin 2\varphi^k)^2} \quad (5)$$

This expression is identical with that of the vector magnitude used by Curray [38], if  $\mathbf{n}$  represents the preferred orientation of the particle. The major principal direction of fabric anisotropy can be obtained by

$$\varphi = \tan^{-1} [2F_{12}/(F_{11} - F_{22})] / 2 \quad (6)$$

Equation (6) results in the magnitude of  $\varphi$  varying in the range of  $-90^\circ$  and  $90^\circ$ . For convention, the  $\varphi$  value can be translated into the range of  $0^\circ$  and  $180^\circ$  with reference to the horizontal axis. In present study, the fabric anisotropy will be quantified by micro-parameters of particle orientation, contact unit normal and branch vector orientation, and their values of intensity  $\Delta$  and major principal direction  $\varphi$  are differentiated by the superscripts  $p$ ,  $c$  and  $b$  respectively.

It is noted that above microstructure based definitions of fabric anisotropy do not have length scale and thus are not per-volume measure, such that proper normalization rules should be followed with respect to the specific volume of the specimens, before they are applied to continuum theory of ACST [13,39]. However, within the main scope of this paper, only undrained tests on specimens with nearly close densities are considered, so obtained measures of the fabric anisotropy could be treated as ‘scaled version’ of those used in the continuum applications.

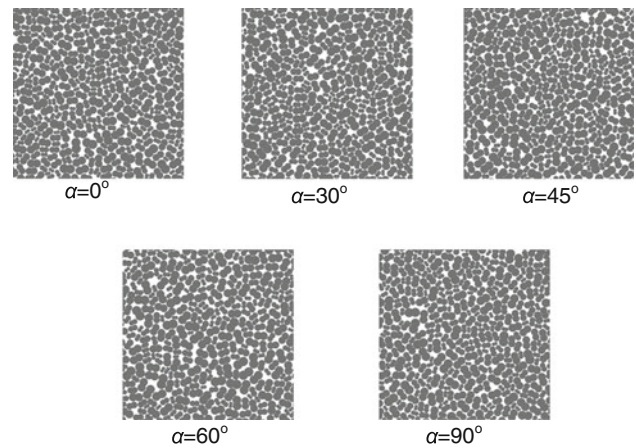


**Fig. 7** Initial configuration of particle assemblage with various bedding angles

As summarized in Table 2, five samples with different bedding angles  $\alpha = 0^\circ, 30^\circ, 45^\circ, 60^\circ$  and  $90^\circ$ , are generated. It is noted that a temporary inter-particle friction  $\mu = 0.35$  is assigned in order to achieve the desired initial density during the deposition under the inclined gravitational acceleration. After that a normal  $\mu = 0.5$  is restored, and the particle assembly is then brought to an equilibrium state. After the isotropic consolidation to 1,000 kPa, all the samples have close initial void ratio, varying in a narrow range of 0.215–0.217, with a mean relatively density  $D_r = \sim 34\%$ , according to Yang et al. [40]. As the spindly clumped element adopted in this study has an identifiable orientation, and the elongated particle tends to lie with its long axis paralleling to the bedding plane. The respective sample configurations for various bedding angles are illustrated in Fig. 7. As shown in Fig. 8, through statistical analysis using Eq. (4), the initial distinct structures/fabrics of samples associated with different bedding angles can be identified. For each bedding angle, it can be seen that there is a trend orientation for the particle orientation, contact unit normal or branch vector orientation. Summarized in Table 2 are the resulting initial fabric anisotropy in terms of particle orientation, contact unit normal and branch vector orientation. It can be seen that the initial preferred particle orientations almost coincide with

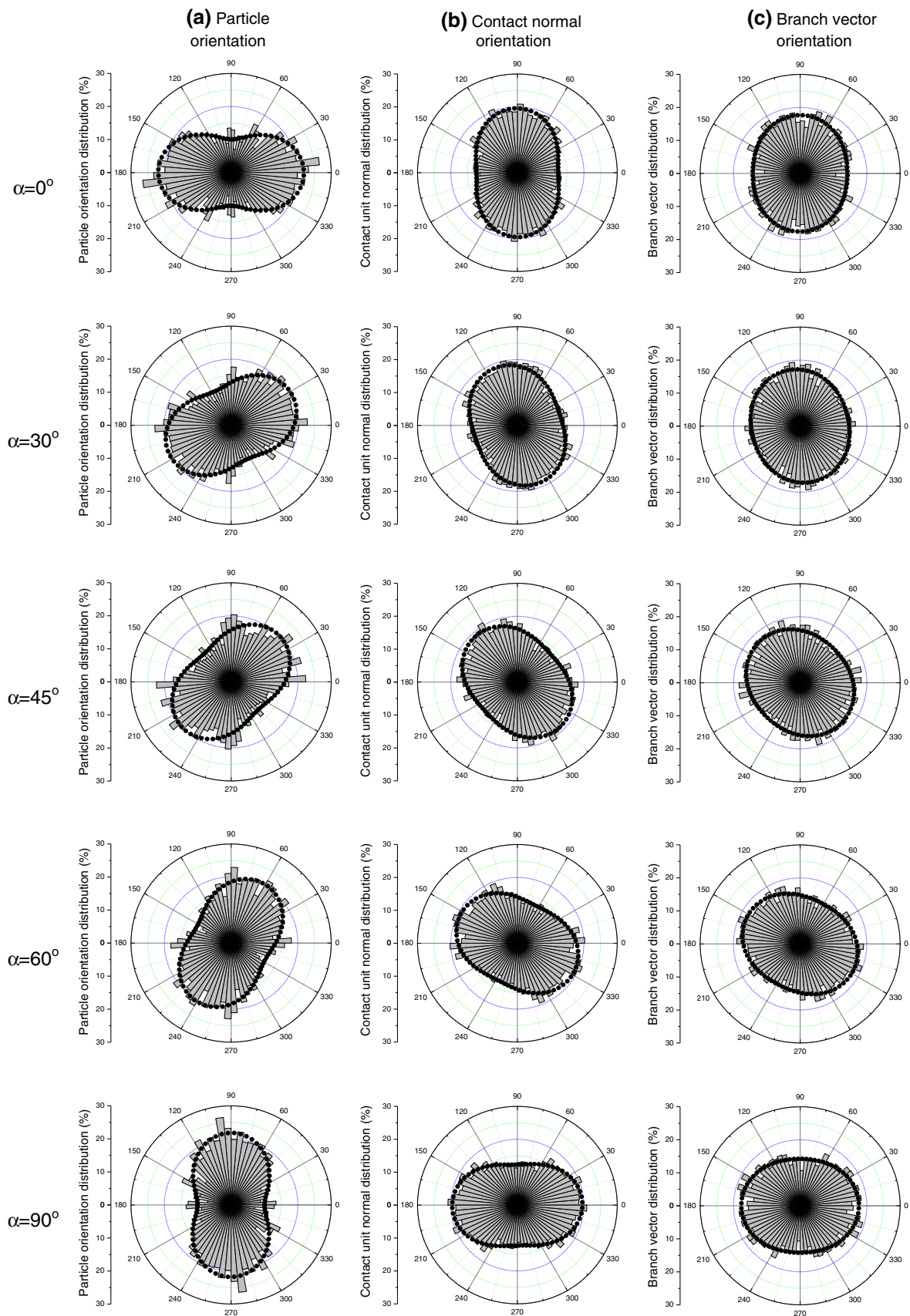


**Fig. 8** Distribution of samples with various bedding angles at initial state

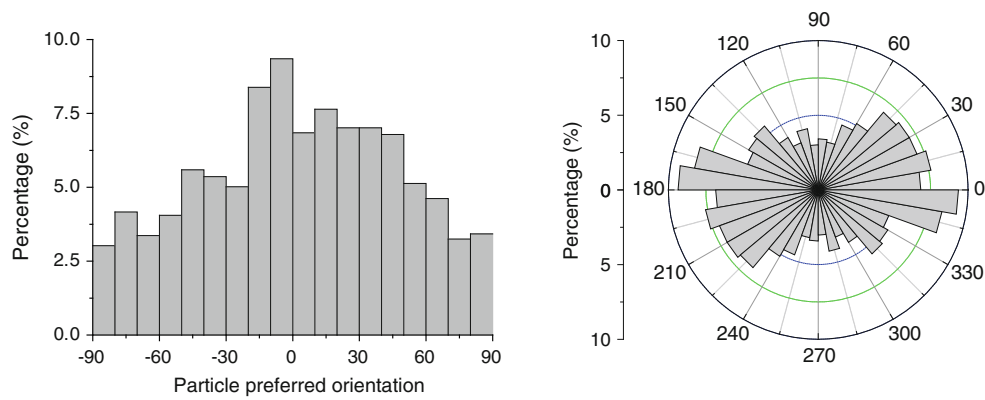
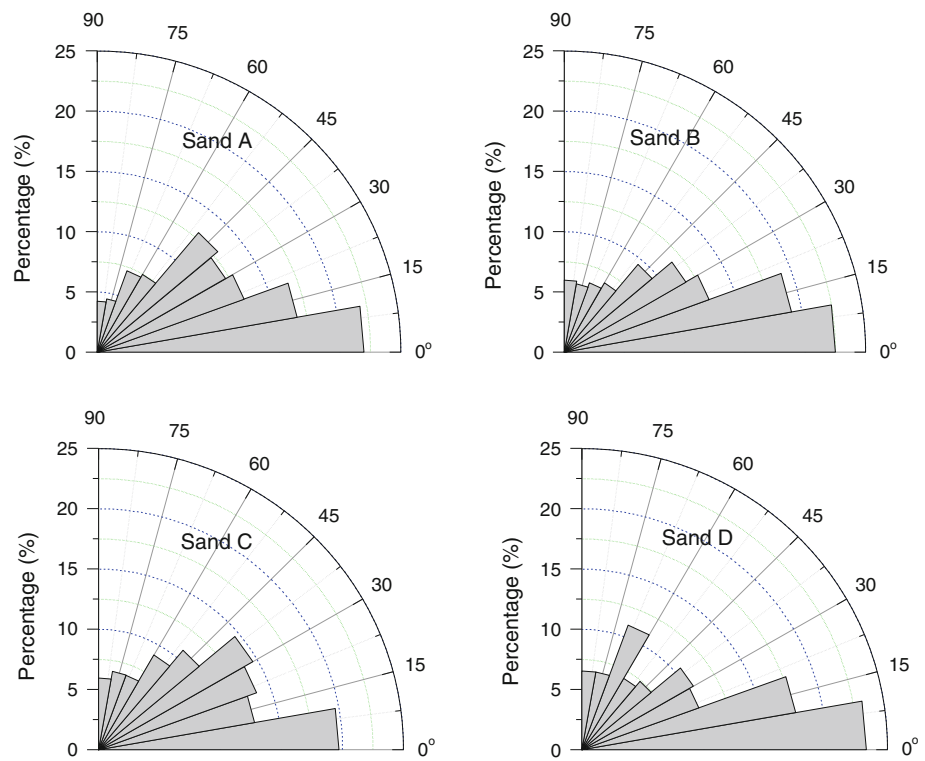


**Fig. 9** Characterization of inherent fabric anisotropy of Toyoura sand with preferred particle orientations for vertical sections (after Yang et al. [5])

**Fig. 10** Contact unit normal ( $\beta$ ) distributions of four different samples (after Oda [41])



the bedding angles (inclination of bedding plane defined in Fig. 1), while those of the contact normal orientation and branch vector orientation are nearly normal to the bedding orientation. As expected, although the samples are generated with different bedding planes, the initial fabric intensities and densities of the samples are varying in a fairly narrow range.

The achieved ‘virtual’ samples can be compared with real samples with sand deposited under gravity in laboratory. Oda [41] prepared the samples by placing the sands layer by layer and then tapping them into desired density. The resulting microstructure of non-spherical sands can be preserved by polyester-resin first and assessed later. Their results show

that the concentration of particle orientation in the bedding plane for the sample prepared by tapping method, similar to that by gravity deposition. Recently a microstructural analysis by Yang et al. [5] adopting the same method on Toyoura sand (composed mainly of angular and elongated particles) sample showed comparable results, see Fig. 9, clearly showing that the sample prepared by dry deposition method has an apparent initial anisotropy with respect to preferred particle orientation distribution, either in the form of histogram or rose diagram. Both experimental observations compare reasonably well with Fig. 8 from the present numerical analysis, suggesting a direct dependence of fabric direction on the bedding plane.

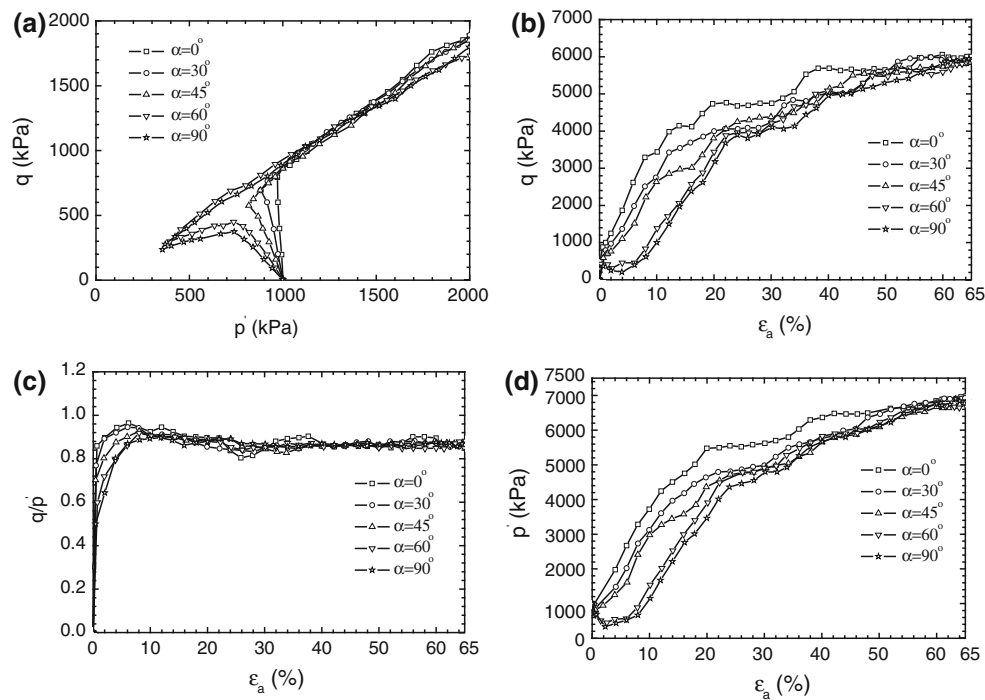


**Fig. 11** Effects of  $\alpha$  on undrained behavior of the granular assembly ( $D_r \sim 34\%$ ). **a**  $q$ - $p'$ . **b**  $q$ - $\varepsilon_a$ . **c**  $q/p'$ - $\varepsilon_a$ . **d**  $p'$ - $\varepsilon_a$

For granular materials, the externally applied loading is transmitted by the force network via contacts between particles. The force chain is dependent not only on the particle geometry that governs the number of contacts for each particle, but also on the contact orientations. To compare with the experimental data, contact normal distributions from Oda [41] are re-plotted into rose diagrams for four different sands, as shown in Fig. 10. It is noted that contact normal  $\beta$  in his study is referenced to the vertical axis. As shown in this figure, the contact unit normal is concentrated in vertical plane, which is perpendicular to the bedding plane for all the four sands.

#### 4 Macroscopic response

A series of undrained biaxial tests were conducted to investigate the mechanical behavior of the five samples with different bedding planes described above. Noting that all the samples have close initial fabric intensity and density except for the fabric directions, the samples can be considered as being rotated with different angles with respect to the loading axes. Recalling that the influence of the fabric anisotropy (not only intensity but also preferred direction) is referenced to the loading directions, the variations in mechanical behavior resulting from the samples with different bedding angles can also reflect the influence arising from the principal stress direction.

Figure 11 presents the mechanical responses of the five ‘loose’ samples with  $e_0 = 0.215$ – $0.217$  of different angles  $\alpha = 0^\circ, 30^\circ, 45^\circ, 60^\circ$  and  $90^\circ$ . Shown in Fig. 11a are the effective stress paths in the  $p'$ - $q$  plane, where  $p' = (\sigma'_x + \sigma'_y)/2$  and  $q = \sigma_x - \sigma_y$ . It can be seen that effective stress paths are different for the samples with various bedding angles. As the inclination of bedding angle  $\alpha$  (with reference to the horizontal direction) increases, the sample transforms from dilatant response into contractant behavior. For  $\alpha = 0^\circ, 30^\circ$  and  $45^\circ$ , the stress-strain behaviors exhibit strong hardening and fairly stable responses, while for  $\alpha = 60^\circ$  and  $90^\circ$ , the samples experience a dominant strain-softening behavior in the early stage of shearing.

Figure 11b shows the stress-strain relationships for the five samples, with  $\varepsilon_a$  denoting the axial strain along  $y$  direction. Despite of the discrepancy on the stress-strain curves, the deviatoric stress at large strain level is flattened off and tends to be stabilized within a narrow band  $\Delta q = \pm 200$  kPa. Shown in Fig. 11c is the development of the mobilized stress ratio of  $q/p'$  against the axial strain. It is found that the five samples have distinct stiffness when  $\varepsilon_a < 10\%$ ; the higher the bedding angle, the smaller the stiffness; when  $\varepsilon_a > 10\%$ , all samples almost converge into a constant stress ratio  $q/p'$  value of  $\sim 0.866$ . As an alternative to Fig. 11a, Fig. 11d presents the evolution of the mean normal effective stress  $p'$  under shearing. It can be seen that  $p'$  value for samples with  $\alpha = 60^\circ$  and  $90^\circ$  drops up to  $\varepsilon_a = 3\%$ , and then picks up with  $\varepsilon_a$  increasing further, while samples with  $\alpha = 0^\circ, 30^\circ$  and

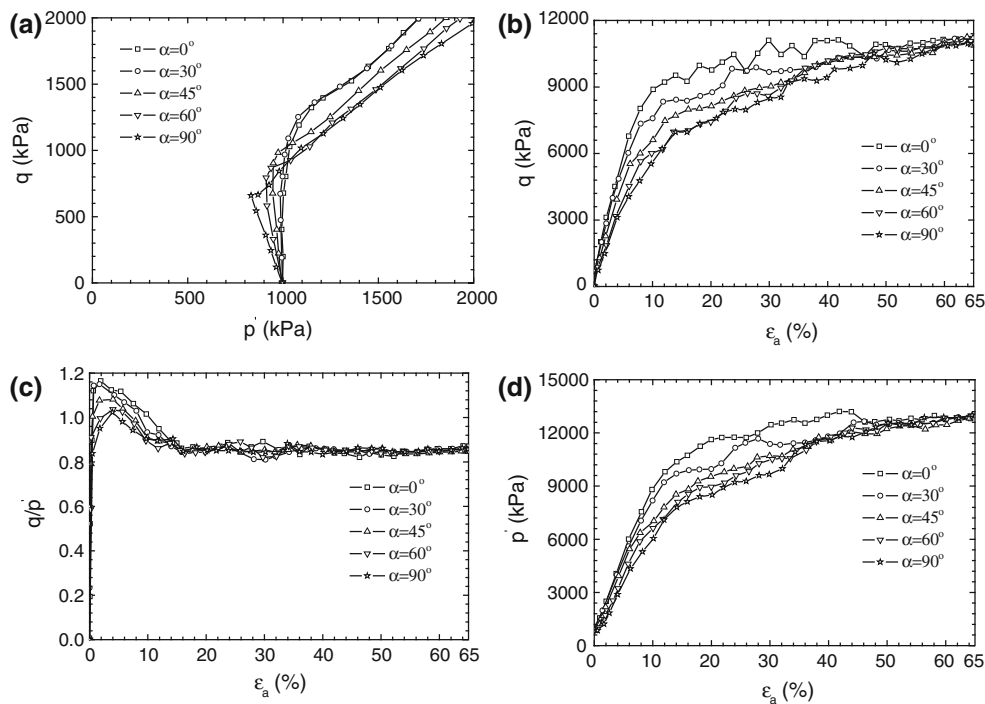


**Fig. 12** Effects of  $\alpha$  on undrained behavior of the granular assembly ( $D_r \sim 64\%$ ). **a**  $q$ - $p'$ . **b**  $q$ - $\epsilon_a$ . **c**  $q/p'$ - $\epsilon_a$ . **d**  $p'$ - $\epsilon_a$

45° exhibit hardening behavior immediately after shearing. It is also noted that the effective stress for all the cases varies within a narrow range  $\Delta p' = \pm 100$  kPa at large strain level  $\epsilon_a \sim 65\%$  and tends to converge to a constant value. This observation suggests the critical state may not be altered by the initial fabric or the stress path (if considering the principal stress direction being rotated with respect to the soil fabric). To verify this finding, another series of tests on ‘medium-dense’ samples with  $e_0 = 0.179$ – $0.181$  ( $D_r \sim 63.6\%$ ) are performed and their responses are shown in Fig. 12. A similar finding of the convergence in  $p'$  and  $q$  for all the five ‘medium-dense’ samples at large strain  $\epsilon_a \sim 65\%$  is noted on Fig. 12b, d, although apparently different behaviors are seen at small strain in Fig. 12a. As shown in Fig. 12c, the  $q/p'$  values flatten off at strain  $\epsilon_a > 15\%$  to a plateau  $\sim 0.856$ , which is very close to that for ‘loose’ samples. This suggests that aforementioned initial fabric independence of critical states is valid for both loose and dense granular media.

The observations above compare reasonably well with experimental results. Oda [15] reported a series of drained triaxial tests performed on samples with different bedding angles and a tendency of the decrease in dilatancy was identified as the bedding angle increases. Yoshimine et al. [2] and Nakata et al. [3] studied the influence of principal stress direction on the undrained response using hollow cylinder tests. In their tests, the principal stress direction was varied with respect to the soil fabric, while maintaining a constant  $b$  value (intermediate stress parameter

$b = (\sigma'_2 - \sigma'_3)/(\sigma'_1 - \sigma'_3)$ ). Both test results confirm the significant effects of principal stress direction on the tendency of dilatancy characteristics of sand.

The dependence of the critical state behavior on the stress path (or shear mode) was also confirmed by experimental tests [1, 3, 42]. Typically as shown recently by Yang et al. [5], identical sand samples subjected to three different stress paths, namely triaxial compression (TC), torsional shear (TS) & triaxial extension (TE), exhibit completely different responses: the specimen in TE is much more contractive than that in TC, with the TS one in between. This difference also implies the anisotropic effect of the orientation of the major principal stress direction, with reference to the deposition plane of the samples. It should be pointed out that the influence of stress paths on the undrained behavior cannot be fully investigated by the present two-dimension analysis, as the influence of the intermediate principal stress may not be considered.

### 5 Microscale observation

To understand the underlying mechanism of fabric anisotropy effects on the overall behavior shown above, the microscopic fabric evolution characteristics are examined for ‘loose’ sample tests shown in Fig. 11. Figure 13 plots the variation of the coordination number  $CN$  against the shear strain for the aforementioned five samples, where  $CN$  is defined as the

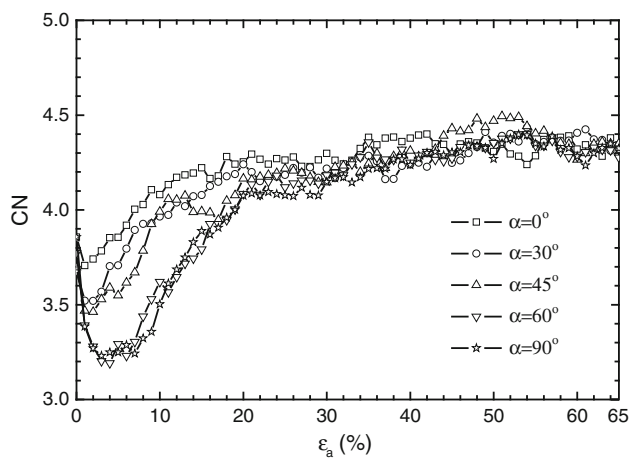


**Fig. 13** Evolution of CN values during the loading

mean contact numbers per particle within a granular assembly. The  $CN$  values decrease at the beginning and then pick up to increase for all cases. For the contractive samples with larger bedding angles  $\alpha = 60^\circ$  and  $90^\circ$ , there is a severe drop in  $CN$  value, while for samples with smaller bedding angles exhibiting more dilative response, a relatively less reduction is observed at the early stage of shear  $\varepsilon_a < 1\%$ . The reduction in the  $CN$  values coincides with the loss of effective mean normal stress, as seen in Fig. 12d, where a contractive behavior dominates before reaching the transformation state [43]. When  $\varepsilon_a > \sim 20\%$ , the  $CN$  values are not appreciably affected by the initial fabric, and tend to converge into a stable value  $\sim 4.3$ .

When the samples are subjected to loading, their macroscopic response is interrelated to the particles interacting through the contacts in the micro-scale. The microstructure changes include the contact anisotropy, particle re-orienting and particle relocating, which are main features of induced anisotropy for granular materials. Evaluation of the microstructure quantities and how they evolve under loading may offer further insights into the overall behaviors stated above. Figure 14 illustrates the evolution characteristic of contact unit normal. Although the major directions of the contact unit normal are differently oriented before shearing, they are gradually re-oriented and their distributions tend to be concentrated in the major principal stress direction (vertical) when  $\varepsilon_a > 4\%$ , irrespective of the initial respective preferred directions. However, the intensities of the contact normal anisotropic distributions are undergone large variations, before approaching a unique value  $\sim 0.42$  at critical state. The general trend of the distributions in contact unit normal shows that the intensity of anisotropy  $\Delta^c$  increases with the shear strain, bringing the samples to more anisotropic states. Shown in Fig. 15 are the distributions of branch vector, which exhibit similar trends to the contact unit normal for both the orientation and the intensity of anisotropic distribution, although less anisotropy intensities (critical value

$0.21 \pm 0.02$ ) are noted as comparing to the contact unit normal ( $\Delta^c < \Delta^b$  at critical state).

Besides the contact unit normal and branch vector orientation, particle re-orientation is another important feature for granular materials. Figure 16 shows the detailed evolution characteristics of anisotropic distributions of preferred particle orientation in both intensity and direction. As is seen in Fig. 16(a), unlike the contact unit normal and branch vector orientation, the variations in the anisotropy intensity of particle orientation span a rather wide range as the loading proceeds. It is interesting to see that for highly contractive case  $\alpha = 90^\circ$ , the intensity  $\Delta^p$  undergoes a significant ‘V’ style variation: as shearing starts, it drops quickly down to nearly zero (a purely isotropic state when  $\Delta^p = 0$ ), then recovers to climb up and join with other cases. At large strain  $\varepsilon_a \sim 65\%$ , the intensity of anisotropy  $\Delta^p$  is converged into a range  $0.54 \pm 0.03$ . Although the initial particle orientations are different for the samples, the particles tend to re-orient to the direction of minor principal stress (horizontal) as the axial strain increases, as shown in Fig. 16b.

## 6 Discussion

According to the classical critical state theory [44,45], critical state is defined as the state where under constant stress the material deforms in shear without volume change, i.e.

$$\dot{p}' = \dot{q} = \dot{\varepsilon}_v = 0 \quad \text{but} \quad \dot{\varepsilon}_q \neq 0, \quad (7)$$

where  $p'$  is the effective mean normal stress,  $q$  the deviatoric stress,  $\varepsilon_v$  the volumetric strain,  $\varepsilon_q$  the deviatoric strain, and a superposed dot signifies the rate. However, based on experimental observations, it has been suggested that a unique critical state, defined in the  $p' - q - e$  (void ratio) space, may exist for soils under shearing, that is, at critical state, both the stress ratio and void ratio (for a given  $p'$ ) are constant, i.e.,

$$(q/p')_c = M \quad \text{and} \quad e = e_c(p') \quad (8)$$

where  $M$  is a material intrinsic coefficient and  $e = e_c(p')$  defines a unique critical state line in the  $e - p'$  plane, with subscript ‘c’ denoting critical state.

The micro-scale analysis shown above suggests that the critical state fabric is highly anisotropic, which has also been widely observed experimentally or numerically [2,3,40,46]. However, as pointed out by Li and Dafalias [13], the classical theory assumes that the critical state itself is independent from the fabric, which is not true and might be directly related to disclose the long debating over the uniqueness of critical state line. Based on thermodynamic theory, Li and Dafalias [13] proposed so called anisotropic critical state theory (ACST), in which the fabric critical value is additional to the requirements set by the classical critical state theory expressed in Eq. (8). That is to say, apart from the

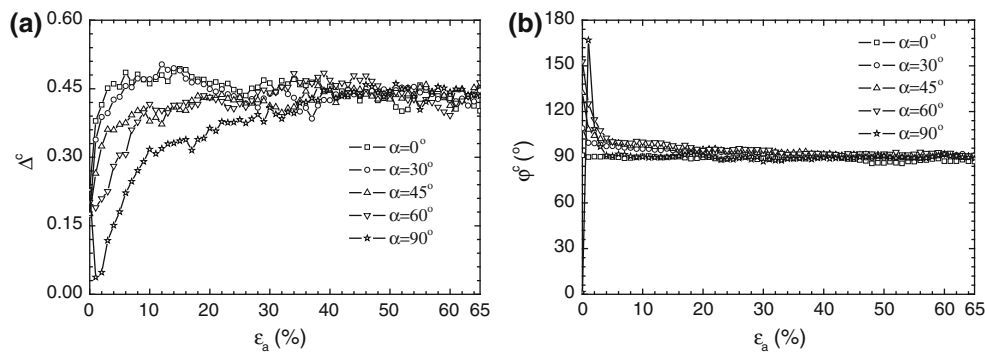


Fig. 14 Evolution of contact unit normal anisotropy (a) intensity (b) preferred orientation

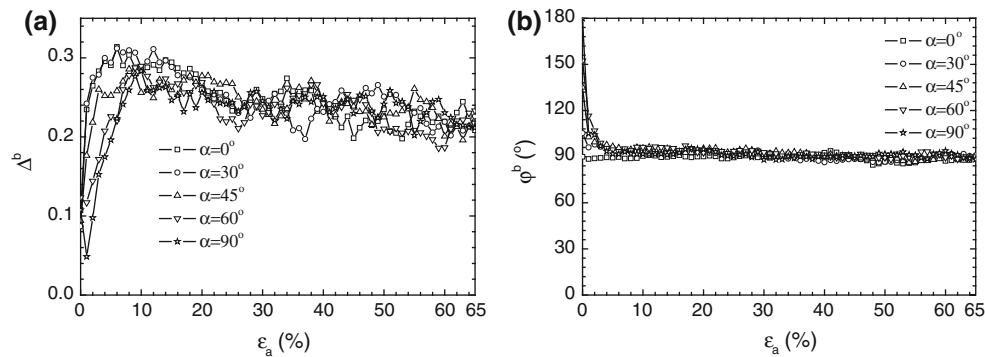


Fig. 15 Evolution of branch vector orientation anisotropy (a) intensity (b) preferred orientation

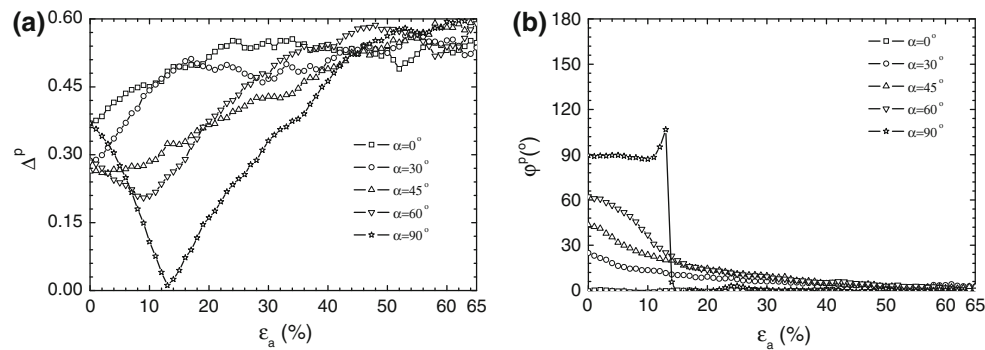


Fig. 16 Evolution of particle orientation anisotropy. a Intensity, b preferred orientation

macroscopic requirements of critical values for the stress and void ratio at critical state, the micro fabric has to also satisfy the critical value.

The numerical examples of biaxial shearing shown above indicate that critical state is unique and also independent of the initial fabric. The uniqueness is not only applied to the stress and strain measurements shown in Fig. 11, but also to the microscopic fabric, see Figs. 13, 14, 15 and 16. However, according to ACST, critical state for a given material is not necessary attainable, with which an example will be illustrated hereafter.

Another sample is generated by deposited under gravity with  $\alpha = 90^\circ$ , and the initial  $e_0 = 0.220$  after the isotropic

consolidation to 1,000 kPa is slightly looser than the samples ( $\bar{e}_0 = 0.216$ ) shown above. An ‘undrained’ biaxial shearing is applied and the effective stress path and stress-strain curve are shown respectively in Fig. 17a, b. Different from the behavior for sample with  $\alpha = 90^\circ$  and  $\bar{e}_0 = 0.216$ , the new sample completely loses its strength and is failed at  $\epsilon_v < 3\%$  with ‘full liquefaction’, as defined in saturated soils. Then a natural question arises, that the sample has reached the critical state yet? Based on numerical analysis on samples with  $e = 0.215\text{--}0.217$ , it is found that all the samples are sheared up to large deformation and terminated at a state satisfying the conditions expressed in Eq. (8) and fabric requirement, which are also proclaimed by ACST. Shown in Fig. 17c is

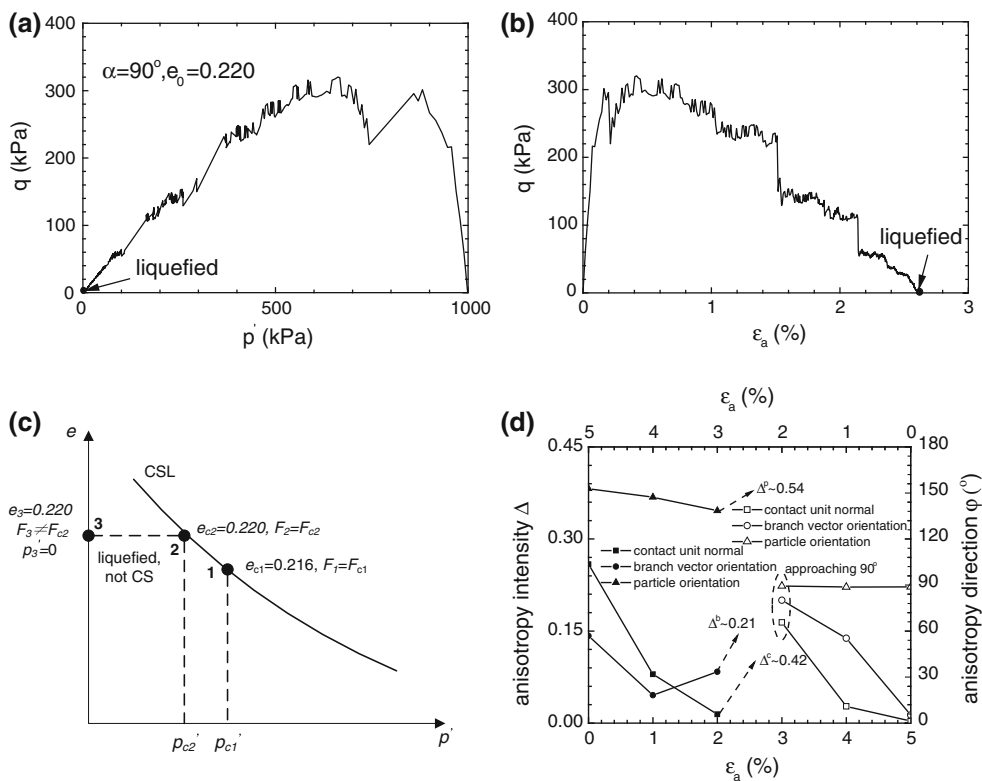


**Fig. 17** Undrained biaxial test for sample with  $\alpha = 90^\circ$  and  $e_0 = 0.216$ . **a**  $q-p$ . **b**  $q-\varepsilon_a$ . **c** Critical state line at  $e-p$  plane. **d** Evolution of anisotropy

a unique critical state line, with Point 1 and Point 2 being critical states for  $e_0 = e_{c1} = 0.216$  and  $e_0 = e_{c2} = 0.220$ , respectively. It is noted that as  $e_{c2}$  is slightly greater than  $e_{c1}$ , the critical state value  $p'_{c2}$  is less than but in the neighboring range of  $p'_{c1}$ . Clearly ‘liquefied’ Point 3 is not a critical state as  $p'_3 = 0 \neq p'_{c2}$ .

However, because Points 1 and 2 are critical states, their fabrics should also satisfy their respective values, i.e.  $F_1 = F_{c1}$  and  $F_2 = F_{c2}$ . We will show that at Point 3, the fabric is also not equal to the critical value, i.e.  $F_3 \neq F_{c2}$ . It is noted from Fig. 13 that critical value of  $CN$  at Point 1  $CN_{c1} \approx 4.2$ , while  $CN_{c2}$  at Point 2 should be varied in Point 1’s neighborhood. But numerical result of sample with  $e_0 = 0.220$  shows that  $CN_3 = 3.0$  at ‘liquefied’ Point 3, much less than required critical value. Shown in Fig. 17d are the fabric evolutions against axial strain  $\varepsilon_a$ , including contact unit normal, branch vector orientation and particle preferred orientation. On this figure, the anisotropy intensity  $\Delta$  is presented with the bottom  $x$  axis and left  $y$  axis coordinate, while the anisotropy direction  $\varphi$  is shown under top  $x$  axis and right  $y$  axis. It is found that although anisotropy directions are more approaching the critical values, the intensities  $\Delta^c$ ,  $\Delta^b$ , and  $\Delta^p$  are far away from their respective critical values, again confirming that ‘liquefied’ state is not a true critical state.

It is known that particle breakage and crushing are inevitably occurred when high stress level is applied to the

granular materials. However, in this paper, particle breakage and crushing are not considered, and the final materials are treated as the same. If particle crushing takes place, the grading of the particles will differ from the original one, and the two materials will be treated as differently, such that their critical state lines will be of course not unique, as elaborated by Wood and Maeda [46], Bandini and Coop [47].

### 7 Incorporating fabric effects and dilatancy into modeling

It has been shown that a dramatic difference exists among the responses of various samples generated with different bedding angles, but sheared under the same biaxial shear stress path. It has also been noted that the principal directions of initial fabrics of the samples are directly related to the bedding angles of particle deposition in the sample generation process, while all samples have almost identical intensity of fabric anisotropy. Figure 18 illustrates the dilatancy characteristics of the sample responses under the biaxial shear, in which dilatancy is defined as  $D = d\varepsilon_v^p/d\varepsilon_q^p$  with subscripts  $v$  and  $q$  denoting volumetric and deviatoric strains respectively, and superscript  $p$  signifying plastic. The dilatancy responses vary with different initial fabrics of the test samples, remarkably before the phase transformation state,

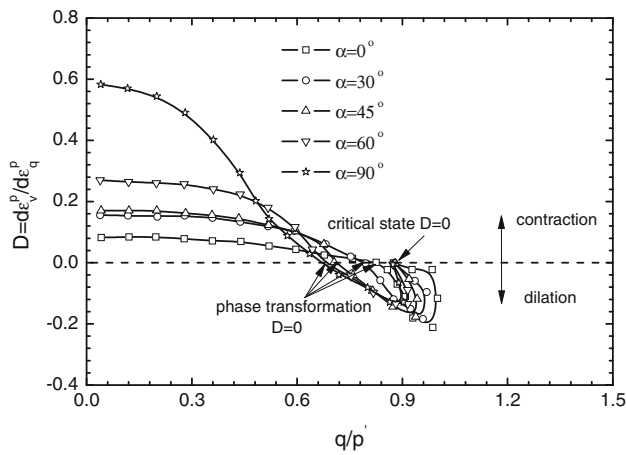


**Fig. 18** Dilatancy against stress ratio

which is a transition state from contraction to dilation [43]. Figure 18 clearly emphasizes that the samples with smaller bedding angles are more dilatant and stiffer, while samples with larger bedding angles exhibit more contractive and soft responses.

In theory, rotating the stress direction on an isotropic soil is the same as simply rotating the reference frame, while rotating the coordination of soil’s fabric is equivalent to the rotating of the stress direction. The elementary framework of plasticity theory is described without explicitly considering fabric anisotropy. For an anisotropic soil, its internal structure or fabric must be described by tensor quantities. That is, its internal variables must include at least one tensor quantity. Assuming we define one symmetric second order tensor,  $\mathbf{F}$ , to describe soil anisotropy, a constitutive equation, say, the yield function, can be expressed as [48]

$$f = f(\boldsymbol{\sigma}, \mathbf{F}) = 0 \tag{9}$$

meaning that the function depends on both the applied stress  $\boldsymbol{\sigma}$  and the material fabric  $\mathbf{F}$ . Based on the representation theory, the objectivity requirements demands that the function must be an isotropic function, i.e., it must be a function of the isotropic invariants of  $\boldsymbol{\sigma}$  and  $\mathbf{F}$ . It follows

$$f = f(J_1, J_{2D}, J_{3D}, K_1, K_{2D}, K_{3D}, L_1, L_2, L_3, L_4) = 0 \tag{10}$$

where  $J_1, J_{2D}$  and  $J_{3D}$  are three invariants of  $\boldsymbol{\sigma}$ ,  $K_1, K_{2D}$  and  $K_{3D}$  are three invariants of  $\mathbf{F}$ , and

$$\begin{cases} L_1 = \boldsymbol{\sigma} : \mathbf{F} \\ L_2 = \boldsymbol{\sigma} : \mathbf{F}^2 \\ L_3 = \boldsymbol{\sigma}^2 : \mathbf{F} \\ L_4 = \boldsymbol{\sigma}^2 : \mathbf{F}^2 \end{cases} \tag{11}$$

are four joint invariants of  $\boldsymbol{\sigma}$  and  $\mathbf{F}$ .

It has been shown that to quantify and simulate the influence of the fabric anisotropy of granular materials objec-

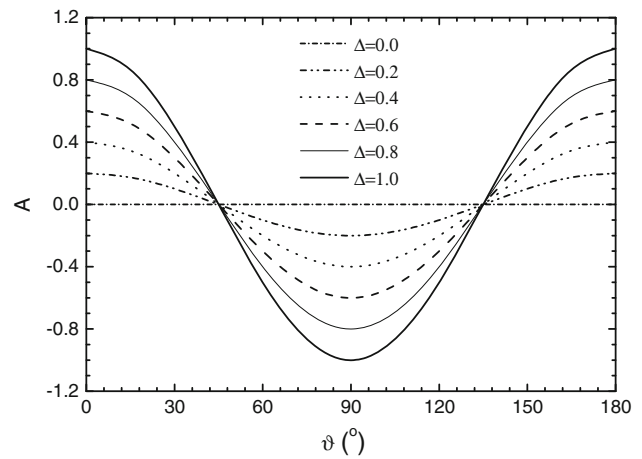


**Fig. 19** Anisotropic state parameter  $A$  versus fabric anisotropy

tively, the loading should be reference to and working conjugatedly with the fabric anisotropy coordinate [5, 9, 14, 49]. In this study, the initial fabric anisotropy and its evolution during the loading process have been identified and quantified, and thus anisotropy effects can be explicitly incorporated into the constitutive model. Considering the scope of this paper, we will illustrate how to link the micro-structures (also their evolutions) with the loading path influences by using the joint tensor and anisotropic parameter.

Under two dimensional conditions, a second-order fabric tensor  $F_{ij}$  in Eq. (3) can be written into a matrix form

$$F_{ij} = \begin{bmatrix} (1 + \Delta)/2 & 0 \\ 0 & (1 - \Delta)/2 \end{bmatrix} \tag{12}$$

in which  $\Delta$  is a descriptor of the intensity of fabric anisotropy in a granular assembly and referring to either initial or induced anisotropy. Consider an orthogonal rotation  $\vartheta$  of the fabric tensor with respect to the horizontal direction, and the new fabric tensor  $\mathbf{F}'$  can be expressed using the transformation equation as

$$F'_{ij} = l_{im}l_{jn}F_{mn} \tag{13}$$

where  $l_{ij} = \cos(x'_i, x_j)$ , the cosine of angle between axes of  $x'_i$  and  $x_j$  with superscript  $'$  denoting rotated coordinate system. The rotated fabric tensor  $\mathbf{F}'$  can be explicitly written into

$$F'_{ij} = \begin{bmatrix} (1 + \Delta \times \cos 2\vartheta)/2 & -\Delta \times \sin \vartheta \cos \vartheta \\ -\Delta \times \sin \vartheta \cos \vartheta & (1 - \Delta \times \cos 2\vartheta)/2 \end{bmatrix} \tag{14}$$

In general, the off-diagonal components of  $F'_{ij}$  do not vanish. In the biaxial shear mode, the stress tensor  $\boldsymbol{\sigma}$  can be expressed as

$$\sigma_{ij} = \begin{bmatrix} \sigma_x & 0 \\ 0 & \sigma_y \end{bmatrix} \tag{15}$$

And its loading direction  $\widehat{\sigma}$  can be represented by the deviatoric part  $\mathbf{s}$  normalized with its module  $|\mathbf{s}|$  as

$$\widehat{\sigma}_{ij} = \frac{1}{\sqrt{2}} \begin{bmatrix} 1 & 0 \\ 0 & -1 \end{bmatrix} \quad (16)$$

It is aware that the stress–strain relation of an anisotropic material will be different if the relative orientation of the material and stress changes. Therefore, the constitutive laws for anisotropic materials must involve non-scalar valued parameters that represent the orientation of the material.

The first joint invariant of loading direction tensor (Eq. 16) and the fabric tensor (Eq. 14) scaled by  $\sqrt{2}$  can be defined as

$$A = \sqrt{2} (\widehat{\sigma}_{ij} : F'_{ij}) = \Delta \times \cos 2\vartheta \quad (17)$$

The index  $A$  is a state parameter, characterizing the anisotropic state in response to the variations either in the initial or the induced fabric anisotropy during the loading process. The variation of the anisotropic state parameter with the fabric anisotropy parameter  $\Delta$  is shown in Fig. 19, where  $\vartheta$  varies from  $0^\circ$  to  $180^\circ$ . It is seen that the  $A$  serves as a state parameter to characterize the influence of the fabric on the mechanical behavior of granular materials under loadings, and in general it may be undergone changes either in magnitude or direction during the loading process. It is noted that if the material is in an isotropic state with  $\Delta = 0$ , the influence of fabric anisotropy vanishes by ensuring the  $A$  value being zero.

Based on the results of numerical simulation, it is found that the dilatancy of the granular assembly depends on the anisotropy, such that it could be explicitly made as a function of anisotropic state parameter  $A$ , to reflect its influence. Similar treatments are also extended and applicable to the plastic modulus and strength, as discussed by Yang et al. [5], Li and Dafalias [14], where the critical state line is no longer unique and assumed as a function of the state parameter, such that the dilatancy is implicitly influence by the anisotropic state. If a unique structure formed at critical state, the corresponding critical state line should be unique, which has been advocated recently by Li and Dafalias [13], and also confirmed earlier by numerical analysis in this study. However, one may assume that the dilatancy is directly related to the anisotropic state, so are plastic modulus and strength if necessary. In general, both the initial and induced anisotropy can be modeled simultaneously by introducing this anisotropic state parameter  $A$ .

## 8 Conclusions

In this paper, a DEM based numerical analysis was reported to simulate the initially anisotropic granular assembly subjected to different principal stress directions with respect to its initial fabric. The numerical samples were achieved by applying inclined gravity acceleration during the particle deposi-

tion, such that the direction of the initial fabric anisotropy was varied with the bedding plane, but with almost the same intensity of fabric anisotropy. The macroscopic responses of the samples under identical bi-axial compression, as well as the induced microstructure changes were further examined, including the contact properties, particle orientation and particle rolling. To reflect and model the anisotropy effects on the dilatancy and other mechanical behavior of granular soil, a general framework based on the joint tensor and anisotropic parameter was introduced in the end. The following conclusions can be drawn from this study.

1. The samples generated by varying gravitational force direction are of different particle preferred orientations, contact unit normals and branch vector orientations. The anisotropy direction of initial fabric is dependent on the bedding angle, while the anisotropy intensity is fairly not affected.
2. The mechanical behaviors and dilatancy of the samples with identical initial conditions except for anisotropy direction may vary dramatically when sheared by biaxial compression under constant volume condition (equivalent to ‘undrained’ condition). The general observations were fairly comparable to the reported experimental results. Nevertheless, both the mean normal effective stress and deviatoric stress at critical state seem to be independent of the initial fabric.
3. Both the contact unit normal and branch vector orientations that represented by the anisotropy intensity and direction were subject to significant variations under shearing. The initial fabric anisotropy tends to be completely erased as deformation progresses, and a unique fabric for the induced anisotropy at critical state was observed both in intensity and direction, which was paralleled to the major principal stress direction. The observations agree reasonably well with existing experimental work. The preferred particle orientation was gradually reoriented to the minor principal stress direction (horizontal) and the results also show that a unique value of fabric anisotropy intensity at critical state.
4. A unique critical state was observed for samples with initially different fabric orientations. In the framework of ACST, the critical state is not only defined to satisfy the conditions of the stress and void ratio required by classical theory, but also has an additional requirement of critical value for fabric anisotropy. The numerical analysis presented in this paper confirmed this point and also showed sample sheared into full ‘liquefaction’ is not a true critical state failure.
5. A general framework was introduced to quantify and model the effects of both the initial and induced anisotropy. A joint tensor in terms of the fabric tensor and deviatoric stress tensor was defined and its invariant  $A$  was

extracted to represent the anisotropic state. In general, the value of  $A$  was varied with the fabric anisotropy in both magnitude and direction. The numerical simulation results suggested that dilatancy, plastic modulus, strength of granular assembly could be made as functions of the anisotropic state parameter  $A$ .

6. Last but not least, given the limitation of the two dimensional analyses, 3-D DEM simulations are more favorite to investigate the critical state behavior of and fabric anisotropy effects on granular materials, such as fabric evolution and critical state quantification, energy dissipation, and loading direction and critical fabric orientation under general stress states, to help to establish a linkage between the micro-scale and continuum level for granular media. More investigations along this line are needed in the future.

**Acknowledgments** The financial support provided by the Research Grants Council (HKU 7191/05E) is acknowledged. The first author is also grateful for support by Natural Science Foundation of China (Nos. 50808159 and 51178421) and project of Zhejiang Education Department (No. N20110091) and Zhejiang provincial natural science foundation (No. Y1110181).

## References

1. Riemer, M.F., Seed, R.B.: Factors affecting apparent position of steady-state line. *J. Geotech. Geoenviron. Eng.* **123**, 281–288 (1997)
2. Yoshimine, M., Ishihara, K., Vargas, W.: Effects of principal stress direction and intermediate principal stress on undrained shear behavior of sand. *Soil Found.* **38**(3), 179–188 (1998)
3. Nakata, Y., Hyodo, M., Yasufuku, N.: Flow deformation of sands subjected to principal stress rotation. *Soil Found.* **38**(2), 115–128 (1998)
4. Yang, Z.X., Li, X.S., Yang, J.: Undrained anisotropy and rotational shear in granular soil. *Géotechnique* **57**(4), 371–384 (2007)
5. Yang, Z.X., Li, X.S., Yang, J.: Quantifying and modelling fabric anisotropy of granular soils. *Geotechnique* **58**(4), 237–248 (2008)
6. Miura, S., Toki, S.: A sample preparation method and its effect on static and cyclic deformation-strength properties of sand. *Soil Found.* **22**(1), 61–77 (1982)
7. Tatsuoka, F., Ochi, K., Fujii, S., Okamoto, M.: Cyclic undrained triaxial and torsional shear strength of sands for different sample preparation methods. *Soil Found.* **26**(3), 23–41 (1986)
8. Vaid, Y.P., Sivathayalan, S., Stedman, D.: Influence of specimen reconstituting method on the undrained response of sand. *Geotech. Test. J.* **22**, 187–195 (1999)
9. Papadimitriou, A.G., Dafalias, Y.F., Yoshimine, M.: Plasticity modeling of the effect of sample preparation method on sand response. *Soil Found.* **40**(2), 109–124 (2005)
10. Arthur, J.R.F., Menzies, B.: Inherent anisotropy in a sand. *Geotechnique* **22**, 115–128 (1972)
11. Been, K., Jefferies, M.G.: A state parameter for sands. *Geotechnique* **35**, 99–112 (1985)
12. Vaid, Y.P., Thomas, J.: Liquefaction and post liquefaction behaviour of sand. *J. Geotech. Eng. ASCE* **121**, 163–173 (1985)
13. Li, X.S., Dafalias, Y.F.: Anisotropic critical state theory: the role of fabric. *J. Eng. Mech. ASCE* **138**, 263–275 (2012)
14. Li, X.S., Dafalias, Y.F.: Constitutive modeling of inherently anisotropic sand behavior. *J. Geotech. Geoenviron. Eng. ASCE* **128**, 868–880 (2002)
15. Oda, M.: The mechanism of fabric changes during compressional deformation of sand. *Soil Found.* **12**(2), 1–18 (1972)
16. Jang, D.J., Frost, J.D., Park, J.Y.: Preparation of epoxy impregnated sand coupons for image analysis. *Geotech. Test. J.* **22**, 147–158 (1999)
17. Muhunthan, B., Masad, E., Assaad, A.: Measurement of uniformity and anisotropy in granular materials. *Geotech. Test. J.* **23**, 423–431 (2000)
18. Oda, M., Konishi, J., Nemat-Nasser, S.: Experimental micromechanical evolution of strength of granular materials: effects of particle rolling. *Mech. Mater.* **1**, 269–283 (1982)
19. Oda, M., Nemat-Nasser, S., Konishi, J.: Stress-induced anisotropy in granular masses. *Soil Found.* **25**(3), 85–97 (1985)
20. Calvetti, F., Combe, G., Lanier, J.: Experimental micromechanical analysis of a 2D-granular material: rotation between structure evolution and loading path. *Mech. Cohesive Frict. Mater.* **2**, 121–163 (1997)
21. Wood, D.A., Leśniewska, D.: Stresses in granular materials. *Granul. Matter* **13**, 395–415 (2011)
22. Chang, C.S., Matsushima, T., Lee, X.: Heterogeneous strain and bounded granular structure change in triaxial specimen studied by computer tomography. *J. Eng. Mech. ASCE* **129**, 1295–1307 (2003)
23. Wang, L.B., Frost, J.D., Lai, J.S.: Three dimensional digital representation of granular material microstructure from X-ray tomography imaging. *J. Comput. Civil Eng. ASCE* **18**, 28–35 (2004)
24. Alshibli, K.A., Alramahi, B.A.: Microscopic evaluation of strain distribution in granular materials during shear. *J. Geotech. Geoenviron. Eng. ASCE* **32**, 80–91 (2006)
25. Oda, M., Kazama, H.: Microstructure of shear bands and its relation to the mechanisms of dilatancy and failure of dense granular soils. *Geotechnique* **48**, 465–481 (1998)
26. Oda, M., Takemura, T., Takahashi, M.: Microstructure in shear band observed by microfocus X-ray computed tomography. *Geotechnique* **54**, 539–542 (2004)
27. Takemura, T., Takahashi, M., Oda, M.: Three-dimensional fabric analysis for anisotropic material using multi-directional scanning line-application to X-ray CT image. *Mater. Trans.* **48**(6), 1173–1178 (2007)
28. Nougier-Lehon, C., Cambou, B., Vincens, E.: Influence of particle shape and angularity on the behaviour of granular materials: a numerical analysis. *Int. J. Numer. Anal. Methods Geomech.* **27**, 1126–1207 (2003)
29. Rothenburg, L., Krut, N.P.: Critical state and evolution of coordination number in simulated granular materials. *Int. J. Solids Struct.* **41**, 5763–5774 (2004)
30. Cheng, Y.P., Bolton, M.D., Nakata, Y.: Grain crushing and critical states observed in DEM simulations. In: García-Rojo, R., Herrmann, H.J., McNamara, S. (eds.) *Powder and Grains*, pp. 1393–1397. Taylor & Francis Group, London (2005)
31. Peña, A.A., García-Rojo, G., Herrmann, H.J.: Influence of particle shape on sheared dense granular media. *Granul. Matter* **9**, 279–291 (2007)
32. Peña, A.A., Lizcano, A., Alonso-Marroquín, F., Herrmann, H.J.: Biaxial test simulations using a packing of polygonal particles. *Int. J. Numer. Anal. Methods Geomech.* **32**, 143–160 (2008)
33. PFC2D User's Manual. Itasca Consulting Group, Inc., Minneapolis, USA (2005)
34. Cundall, P.A., Strack, O.D.L.: A discrete numerical model for granular assemblies. *Geotechnique* **29**, 47–65 (1979)
35. Ishihara, K.: *Soil Behavior in Earthquake Geotechnics*. Oxford Science, Oxford (1996)

36. Yimsiri, S., Soga, K.: Effects of soil fabric on behaviors of granular soils: microscopic modeling. *Comput. Geotech.* **38**, 861–874 (2011)
37. Oda, M.: Fabric tensors and its geometrical meaning. In: Oda, M., Iwashita, K. (eds.), *Introduction to Mechanics of Granular Materials*. Balkema, Rotterdam, pp. 27–35 (1999)
38. Curray, J.R.: Analysis of two-dimensional orientation data. *J. Geol.* **64**, 117–131 (1956)
39. Li, X.S., Dafalias, Y.F.: A thermodynamic perspective of fabric enhanced critical state soil mechanics and the uniqueness of critical state line. In: *Third International Workshop on Modern Trends in Geomechanics IW-MTG3*, UK, pp. 4–6 (2012)
40. Yang, Z.X., Yang, J., Wang, L.Z.: On the influence of inter-particle friction and dilatancy in granular materials: a numerical analysis. *Granul. Matter* **14**(3), 433–447 (2012)
41. Oda, M.: Initial fabrics and their relations to mechanical properties of granular material. *Soil Found.* **12**(1), 17–36 (1972)
42. Vaid, Y.P., Chern, J.C.: Cyclic and monotonic undrained response of sands. In: *Proceedings of the ASCE Convention in Advances in the Art of Testing Soils Under Cyclic Loading Conditions*, Detroit, pp. 120–147 (1985)
43. Ishihara, K., Tatsuoka, F., Yasua, S.: Undrained deformation and liquefaction of sand under cyclic stresses. *Soil Found.* **15**(1), 29–44 (1975)
44. Roscoe, K.H., Schofield, A.N., Wroth, C.P.: On the yielding of soils. *Geotechnique* **8**(1), 22–53 (1958)
45. Schofield, A.N., Wroth, C.P.: *Critical state soil mechanics*. McGraw-Hill, London (1968)
46. Wood, D.M., Maeda, K.: Changing grading of soil: effect on critical states. *Acta Geotech.* **3**, 3–14 (2008)
47. Bandini, V., Coop, M.R.: The influence of particle breakage on the location of the critical state line of sands. *Soil Found.* **51**(4), 591–600 (2011)
48. Li, X.S., Yang, Z.X.: Sand response beyond triaxial space—torsional testing. In: *25th National Geotechnical Testing Symposium*, Hangzhou, China, pp. 24–34 (2008)
49. Tobita, Y.: Contact tensor in constitutive model for granular materials. In: Satake, M., Jenkins, J. (eds.) *Proceedings of the US–Japan Seminar on Micromechanics of Granular Materials*, Sendai-Zao, Japan. Elsevier, New York, pp. 263–270 (1988)